

Investigating the elliptic anisotropy of identified particles in p–Pb collisions with a multi-phase transport model

Siyu Tang,¹ Liang Zheng,^{2,*} Xiaoming Zhang,^{3,†} and Renzhuo Wan^{4,5,‡}

¹*School of Mathematical and Physical Sciences,
Wuhan Textile University, Wuhan 430200, China*

²*School of Mathematics and Physics, China University of Geosciences (Wuhan), Wuhan 430074, China*

³*Key Laboratory of Quark and Lepton Physics (MOE) and Institute of Particle Physics,
Central China Normal University, Wuhan 430079, China*

⁴*Hubei Key Laboratory of Digital Textile Equipment,
Wuhan Textile University, Wuhan 430200, China*

⁵*School of Electronic and Electrical Engineering,
Wuhan Textile University, Wuhan 430200, China*

(Dated: May 19, 2023)

The elliptic azimuthal anisotropy coefficient (v_2) of identified particles at midrapidity ($|\eta| < 0.8$) is investigated in p–Pb collisions at $\sqrt{s_{NN}} = 5.02$ TeV using the multi-phase transport model (AMPT). The calculations of differential v_2 , based on the advanced flow extraction method, of light flavor hadrons (pions, kaons, protons and Λ) in small collision systems are extended to a wider transverse momentum (p_T) range of up to 8 GeV/c for the first time. The string melting version of the AMPT model provides a good description of the measured p_T -differential v_2 of mesons but exhibits a slight deviation from the baryon v_2 . In addition, we observe the features of mass ordering at low p_T and approximate number of constituent quark (NCQ) scaling at intermediate p_T . Moreover, we demonstrate that hadronic rescattering does not have a significant impact on v_2 in p–Pb collisions for different centrality selections, while partonic scatterings dominate in generating the elliptic anisotropy of the final particles. This study provides further insight into understanding the origin of collective-like behaviors in small collision systems, and has referential value for future measurements of azimuthal anisotropy.

Keywords: Azimuthal anisotropy, Small collision systems, Transport model

I. INTRODUCTION

The main goal of the heavy-ion collisions at ultra-relativistic energies is to explore the deconfined state of strongly-interacting matter created at high energy density and temperature, known as the quark-gluon plasma (QGP)[1, 2]. One of the important observables to investigate the transport properties of the QGP is the anisotropic flow[3, 4], which is quantified by the flow harmonic coefficients v_n obtained from the Fourier expansion of the azimuthal distribution of produced particles[5, 6], as

$$\frac{dN}{d\varphi} \propto 1 + 2 \sum_{n=1}^{\infty} v_n \cos[n(\varphi - \Psi_n)], \quad (1)$$

where φ is the azimuthal angle of the final-state particle angle and Ψ_n is the symmetry-plane angle in the collision for the n -th harmonic[7, 8]. The second order coefficient, v_2 , referred to elliptic flow, is derived from the initial state spatial anisotropy of the almond-shaped collision overlap region being propagated to the

final state momentum space. The magnitude of elliptic flow is sensitive to the fundamental transport properties of the fireball, such as the temperature dependent equation of state and the ratio of shear viscosity to entropy density (η/s)[9, 10].

In past decades, various measurements of elliptic flow in heavy-ion collisions performed at the Relativistic Heavy Ion Collider (RHIC)[11–14] and the Large Hadron Collider (LHC)[15–18] help to build a full paradigm of the strongly-coupled QGP. These studies indicate that the QGP behaves like a nearly perfect fluid according to the comparison between the extracted η/s and hydrodynamic calculations. In addition, wide measurements of p_T -differential elliptic flow for identified particles are performed in ALICE[19, 20]. The observed mass-ordering effect (i.e. heavier particles have smaller elliptic flow than that of lighter particles at same p_T) at low p_T is well described by hydrodynamic calculations, which attributes to the radial expansion of the QGP. At intermediate p_T , the grouping of v_2 of mesons and baryons is observed, with mesons exhibiting less v_2 than baryons. These behaviours can be explained by the hypothesis that baryon and meson have different production mechanisms through quark coalescence, which was further investigated using the number of constituent quarks (NCQ) scaling[21, 22]. Interestingly, such flow-like phenomena are also found in small colli-

* Correspondence email address: zhengliang@cug.edu.cn

† Correspondence email address: xiaoming.zhang@ccnu.edu.cn

‡ Correspondence email address: wanrz@wtu.edu.cn

sion systems, where no QGP is expected to be formed. The long-range double ridge structures were firstly observed for identified light and strange hadrons in high-multiplicity pp and p-Pb collisions by the ALICE, ATLAS and CMS collaborations, associated with the discovery of a significant positive v_2 [23–26]. The observed particle-mass dependence of v_2 is similar to those measured in heavy-ion collisions[26], however the origin of such collective-like behavior is still not clear. Several theoretical explanations relying on either initial-state or final-state effects were proposed to understand the origin of azimuthal anisotropies in small systems. The studies extending hydrodynamics from large to small systems based on the final-state effects can well describe the v_2 of soft hadrons[27–29], however they are based on a strong assumption that there are enough scatterings among constituents in small systems. The Color-Glass Condensate (CGC) based models and the IP-Glasma models considering the effect of momentum correlations in the initial state can quantitatively describe some features of collectivity in p-Pb collisions[30, 31], but without clear conclusions, particularly regarding the dependence on collision systems and rapidity. In addition, an approach called parton escape shows that few scatterings can also create enough azimuthal anisotropies, which was investigated with the multi-phase transport (AMPT)[32, 33]. The v_2 of light hadrons measured in p-Pb collisions are well described in AMPT, where the contribution of anisotropic parton escape instead of hydrodynamics plays an important role[33].

In this study, we extend the AMPT calculations of the p_T -differential v_2 for identified particles (π^\pm , K^\pm , $p(\bar{p})$, $\Lambda(\bar{\Lambda})$) to higher p_T region in p-Pb collisions at 5.02 TeV, in order to systematically test the mass-ordering effect and baryon-meson grouping at low- and intermediate- p_T , respectively. We also investigate how the key mechanisms implemented in AMPT, such as the parton cascade and hadronic rescattering, work on the elliptic anisotropy in small collision systems. In addition, various nonflow subtraction methods with different sensitivities to jet-like correlations are studied in this work.

II. MODEL AND METHODOLOGY

A multiphase transport model

The string melting version of the AMPT model (v2.26t9b, available online)[32, 34] is employed in this study to calculate the v_2 of final-state particles in high-multiplicity p-Pb at 5.02 TeV. Four main processes are included in AMPT model: the initial conditions, the parton scatterings, the hadronization and the hadronic interactions. The initial conditions are generated from the heavy ion jet interaction genera-

tor (HIJING) model[35, 36], where the minijet partons and soft-excited string are produced, then they are converted to primordial hadrons based on the Lund fragmentation. Under the string melting mechanism, these primordial hadrons are melted into partons according to their flavor and spin structures. Elastic scatterings between the partons are simulated using the Zhang's parton cascade (ZPC) model[37], which includes two-body scatterings with the cross section described by the following simplified equation:

$$\sigma_{gg} \approx \frac{9\pi\alpha_s^2}{2\mu^2}. \quad (2)$$

In this paper, the strong coupling constant α_s is set to 0.33 and the Debye screening mass $\mu = 2.2814 \text{ fm}^{-1}$, resulting the total parton scattering cross section is $\sigma = 3 \text{ mb}$. To isolate the effect of partonic scattering, the σ is also set to be close to 0 by increasing μ in this work (see set "w/o parton scat." in Tab. I). Once partonic interaction ceases, the hadronization with a quark coalescence model is implemented to combine nearest two (or three) quarks into mesons (or baryons) [32]. The formed hadrons enter the subsequent hadronic rescattering process using a relativistic transport (ART) model [38], where both elastic and inelastic scatterings are considered for baryon-baryon, baryon-meson, and meson-meson interactions. The hadronic interactions time is set by default to $t_{max} = 30 \text{ fm/c}$. Alternatively, t_{max} is set to 0.4 fm/c to effectively turns off the hadron scattering process while still considering the resonance decay[39](see set "w/o hadron scat." in Tab. I). In addition, the random orientation of reaction plane is turn on and the shadowing effect is considered in this analysis.

Table I. Details of three configurations

Description	$\sigma(\text{mb})$	$t_{\text{max}}(\text{fm/c})$
w/ all	3	30
w/o parton scat.	~ 0	30
w/o hadron scat.	3	0.4

Two-particle correlation and nonflow subtraction

The two-particle correlation method (2PC) is widely used to extract the flow signal in small collision system since it has great power to suppress the nonflow contribution from the long-range jet correlations. Similar to Eq. 1, the azimuthal correlation between two emission particles can be represented by N^{pairs} pair of emitted particles (labeled as $C(\Delta\varphi)$) as a function of relative

angle $\Delta\varphi = \varphi^a - \varphi^b$ between particle a and particle b and expanded in Fourier series as:

$$C(\Delta\varphi) = \frac{dN^{\text{pair}}}{d\Delta\varphi} \propto 1 + 2 \sum_{n=1}^{\infty} V_{n\Delta}(p_T^a, p_T^b) \cos[n(\Delta\varphi)], \quad (3)$$

where $V_{n\Delta}$ refers to the two-particle n -th order harmonic. In a pure hydrodynamic picture, since the particle emission is independent, the $V_{n\Delta}(p_T^a, p_T^b)$ can be factorized into product of single particle flow v_n^a and v_n^b :

$$V_{n\Delta}(p_T^a, p_T^b) = v_n(p_T^a) v_n(p_T^b). \quad (4)$$

Based on the factorization assumption, the v_n of single particle a can be obtained with so-called 3×2PC method, which was recently proposed in PHENIX Collaboration[40]. It requires to form the two-particle correlations between three groups of particles (labeled as a , b and c) and extract the flow coefficients for three combinations:

$$v_n(p_T^a) = \sqrt{\frac{V_{n\Delta}(p_T^a, p_T^b) V_{n\Delta}(p_T^a, p_T^c)}{V_{n\Delta}(p_T^b, p_T^c)}}. \quad (5)$$

In small collision systems, the main nonflow contribution to the flow signal originates from jet correlations. These correlations are typically classified into two categories: the near-side jet and the away-side jet (dijet). To subtract the former, a large rapidity gap between trigger and associated particles is often introduced during the construction of correlations. On the other hand, several methods have been developed to suppress the latter. One traditional approach is directly subtracting the correlation function distribution obtained from low-multiplicity events[24], commonly referred to as "peripheral collisions," from that obtained from high-multiplicity events, or "central collisions." This method assumes that the yield and shape of dijets are identical in both types of collisions, as shown:

$$\begin{aligned} C^{\text{HM}}(\Delta\varphi) - C^{\text{LM}}(\Delta\varphi) &\propto 1 + 2 \sum_{n=1}^{\infty} V_{n\Delta} \cos[n(\Delta\varphi)] \\ &= a_0 + 2 \sum_{n=1}^{\infty} a_n \cos[n(\Delta\varphi)], \end{aligned} \quad (6)$$

where $C^{\text{HM}}(\Delta\varphi)$ and $C^{\text{LM}}(\Delta\varphi)$ represent the correlation function distribution obtained in low- and high-multiplicity events, respectively. This method relies on the "zero yield at minimum" (ZYAM) hypothesis[24] that a flat combinatoric component should be subtracted from the correlation function in low-multiplicity events. So the fit parameter a_2 is the absolute modulation in the subtracted correlation function distribution and characterizes a modulation relative to a baseline

assuming that such a modulation is not present in the low-multiplicity class below the baseline. In this case, the flow coefficient $V_{n\Delta}$ is calculated as:

$$V_{n\Delta} = a_n / (a_0 + b), \quad (7)$$

where b is the baseline estimated at the minimum of correlation function in low-multiplicity events. However the measurement of jet-like correlations in p-Pb collisions indicates that the dependence of dijet yield on particle multiplicity can not be ignored. In this case, a new template fit method is developed by the ATLAS collaboration[41], where the correlation function distribution obtained in high-multiplicity events, is assumed to result from a superposition of the distribution obtained in low-multiplicity events scaled up by a multiplicative factor F , and a constant modulated by $\cos(n\Delta\varphi)$ for $n > 1$, as shown in:

$$C(\Delta\varphi) = F C^{\text{LM}}(\Delta\varphi) + G(1 + 2 \sum_{n=1}^3 V_{n\Delta} \cos(n\Delta\varphi)), \quad (8)$$

where G is the normalization factor to keep the integral of $C(\Delta\varphi)$ is equal to $C^{\text{HM}}(\Delta\varphi)$. Furthermore, an improved template fit method [42] developed in recent years is also tested in this work. It applies a correction procedure on the default template fit method by considering the multiplicity dependence of remaining ridge in low-multiplicity events, as shown in:

$$V_{n\Delta} = V_{n\Delta}(\text{tmp}) - \frac{F G^{\text{LM}}}{G^{\text{HM}}} (V_{n\Delta}^2(\text{tmp}) - V_{n\Delta}^2(\text{LM})), \quad (9)$$

where the $V_{n\Delta}(\text{tmp})$ and $V_{n\Delta}^2(\text{LM})$ are obtained with default template method in high- and low-multiplicity events. All these nonflow subtraction methods are implemented in this work, and their different sensitivities on nonflow effect are also discussed in this paper.

III. ANALYSIS PROCEDURES

In order to compare the AMPT calculations with the results from ALICE directly, we focus on the particles are selected at pseudorapidity range $|\eta| < 0.8$ which is same as the TPC acceptance in ALICE. In 3×2PC method, the long-range correlations are constructed between the charged particles at midrapidity, forward rapidity ($2.5 < \eta < 4$) and backward rapidity ($-4 < \eta < -2.5$), i.e. the central-forward correlation ($-4.8 < \Delta\eta < -1.7$), central-backward correlation ($1.7 < \Delta\eta < 4.8$) and backward-forward correlations ($-8 < \Delta\eta < -5$). In addition, the centrality classes are defined counting charged particles in the acceptance of the V0A detector[43], i.e. in $2.8 < \eta < 5.1$.

The correlation function distribution $C(\Delta\varphi)$ is obtained by correcting the number of particle-pairs in

same events normalized to the number of trigger particles N_{trig} with event-mixing technique[41], as:

$$C(\Delta\varphi, \Delta\eta) = \frac{1}{N_{\text{trig}}} \frac{d^2 N_{\text{pairs}}}{d\Delta\eta d\Delta\varphi} = \frac{S(\Delta\varphi, \Delta\eta)}{B(\Delta\varphi, \Delta\eta)}, \quad (10)$$

where $S(\Delta\varphi, \Delta\eta) = \frac{1}{N_{\text{trig}}} \frac{d^2 N_{\text{same}}}{d\Delta\eta d\Delta\varphi}$ is the correlation function in same events and $B(\Delta\varphi, \Delta\eta) = \alpha \frac{d^2 N_{\text{mixed}}}{d\Delta\eta d\Delta\varphi}$ is the associated yield as a function of $\Delta\varphi$ and $\Delta\varphi$ in mixed events. The factor α is used to normalize the $B(\Delta\varphi, \Delta\eta)$ to unity in the $\Delta\eta$ region of maximal pair acceptance. The obtained 2-D correlation function $C(\Delta\varphi, \Delta\eta)$ is projected into $\Delta\varphi$ axis, then we follow the nonflow subtraction procedures and factorization as discussed in Eq. 5–Eq. 9, the v_2 of charged particles at $|\eta| < 0.8$ can be calculated.

IV. RESULTS AND DISCUSSIONS

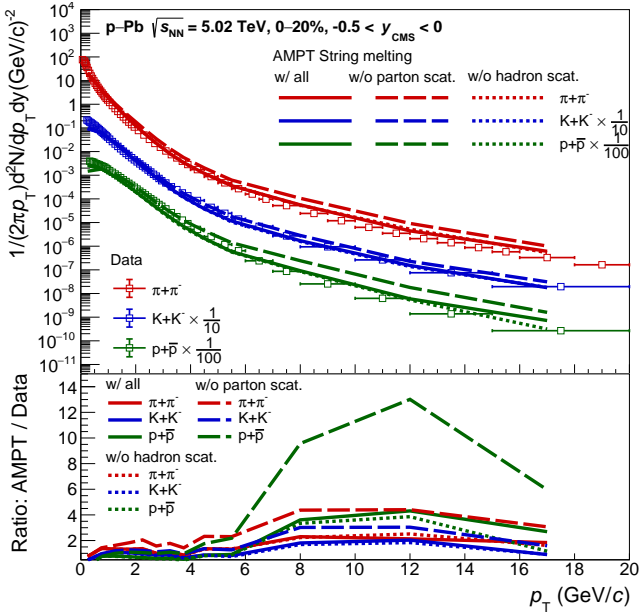


Figure 1. The p_T distribution of pions, kaons and protons in 0–20% high-multiplicity p–Pb collisions at $\sqrt{s_{\text{NN}}} = 5.02$ TeV, obtained from AMPT model calculations, is compared to ALICE measurement. The results in AMPT without hadronic scattering and partonic scattering are also presented.

We firstly investigate the p_T spectrum of identified particles before performing the flow analysis. Figure 1 illustrates the p_T distribution of proton, pion and kaon in 0–20% high-multiplicity p–Pb collisions at $\sqrt{s_{\text{NN}}} = 5.02$ TeV, which are obtained from AMPT with three

different sets of configurations listed in Tab. I, and ALICE experimental data. The AMPT results with and without considering hadronic rescatterings are consistent with each other. This behavior is different from the previous findings in heavy-ion collisions where the hadronic interaction reduce the particle yield significantly [44]. The spectrum obtained in AMPT without considering the parton cascade process is enhanced compared to that with partonic scattering, and such enhancement is more significant at high p_T . This outcome is expected, as partons experience energy loss during the parton cascade, which reduces the production of final-state particles. In addition, the ratios of the p_T spectra obtained from AMPT calculations and data are also shown. The AMPT model calculation reproduces the low and intermediate p_T data well when both partonic and hadronic scattering are included, however it overestimates the high p_T data, as parton-parton inelastic collisions and subsequently hard parton fragmentation are absent in model [34].

Figure 2 (left) shows the v_2 of pions, kaons, protons and Λ as a function of p_T in 0–20% high-multiplicity p–Pb collisions at $\sqrt{s_{\text{NN}}} = 5.02$ TeV, obtained in AMPT calculations with 3×2PC method. The comparison with the ALICE measurement for the v_2 of charged hadrons, pions, kaons and protons, and the CMS measurement for the v_2 of K_s^0 and Λ , is also presented. The AMPT calculations applied the template fit method to suppress the away-side jet contribution and considered the ZYAM assumption to enable a direct comparison with the observed data. A positive v_2 of charged hadrons, pions, kaons, protons and Λ is observed in AMPT calculations, and the mass-ordering effect (i.e. the v_2 of baryons is lower than that of mesons) is also reproduced for $p_T < 2$ GeV/c. Thanks to the advanced flow extraction method, calculations of v_2 are extended to high p_T region, up to 8 GeV/c in the AMPT model for the first time. The v_2 of protons and Λ are consistent, and both of them are observed to have a higher value of v_2 compared to that of mesons for $2 < p_T < 7$ GeV/c. This meson-baryon particle type grouping, observed in heavy-ion collisions flow measurement, is an indication of the collective behavior at the partonic level followed by the coalescence of quarks into hadrons. The number of constituent quarks (NCQ) scaling technique, described in [21], can be used for further studies on this grouping. The v_2 and p_T in Fig. 2 (left) are replaced by v_2/n_q and p_T/n_q , where the n_q is the number of constituent quark in mesons ($n_q = 2$) and baryons ($n_q = 3$), as shown in Fig. 2 (right). The v_2/n_q obtained from data shows approximate values at intermediate p_T , but the results calculated in AMPT can not reproduce the scaling in $p_T/n_q > 1$ GeV/c. In order to consider the observed mass hierarchy of v_2 , we also plot the v_2 of identified particle as a function of the transverse kinetic energy kE_T ($kE_T = m_T - m_0 = \sqrt{p_T^2 + m_0^2} - m_0$),

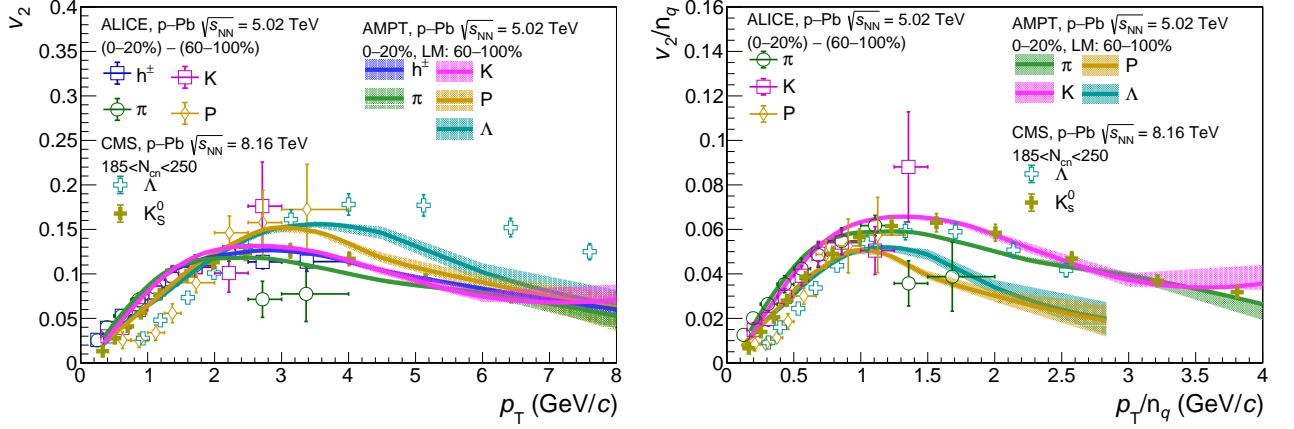


Figure 2. Left: the v_2 as a function of p_T in 0-20% high-multiplicity p-Pb collisions at $\sqrt{s_{NN}} = 5.02$ TeV, obtained from default AMPT model calculations with $3 \times 2PC$ method, is compared to ALICE and CMS measurement. Right: the p_T -differential v_2 scaled by the number of constituent quark (n_q).

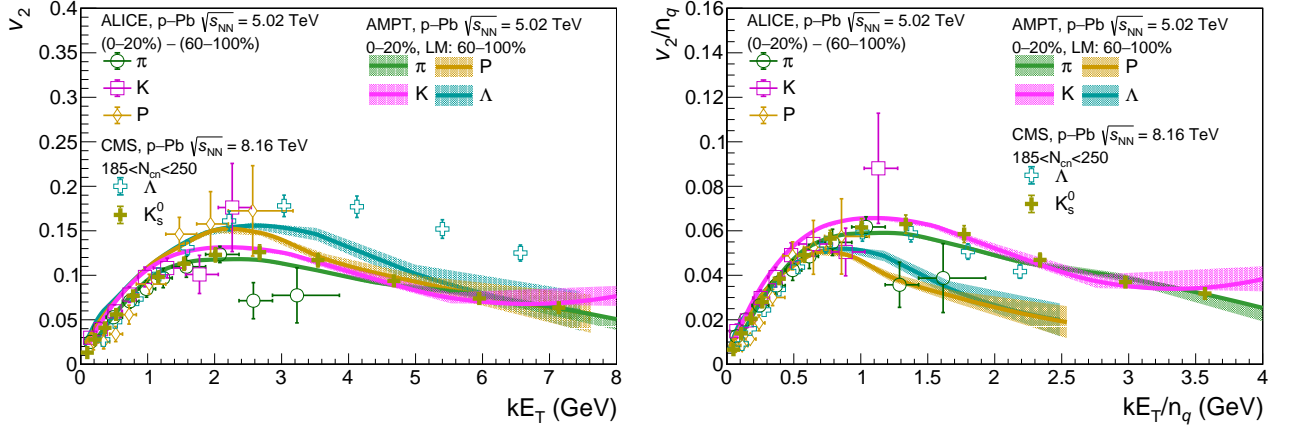


Figure 3. Left: the v_2 as a function of transverse kinetic energy (kE_T) in 0-20% high-multiplicity p-Pb collisions at $\sqrt{s_{NN}} = 5.02$ TeV, obtained from default AMPT model calculations with $3 \times 2PC$ method, is compared to ALICE and CMS measurement. Right: the kE_T -differential v_2 scaled by the number of constituent quark (n_q).

and its NCQ scaling in Fig. 3 (left) and Fig. 3 (right). All particle species show a set of similar v_2 values after the NCQ scaling in $kE_T/n_q < 1$ GeV, confirming that the quark degree of freedom in the flowing matter can be also probed in transport model. However such NCQ scaling is violated for $kE_T/n_q > 1$ GeV. It may be attributed to the hadronization mechanism implemented in current AMPT version, where the baryons are produced only after the formation of meson according simply combining three nearest partons regardless of the relative momentum among the coalescing partons [45]. More studies on v_2 calculations in small collision systems with improved quark coalescence model in AMPT need to be performed in the future.

We also examine the integrated v_2 in several central-

ity bins between 0-60% for $0.4 < kE_T < 1$ GeV where the NCQ scaling is satisfied, as shown in Fig. 4 (top). The nonflow contribution is still estimated in 60-100% centrality class and subtracted with template fit method. It is found that the v_2 values decrease from central to peripheral collisions, and show a clear mass splitting for baryon and meson. In addition, the ratio of n_q scaled integrated v_2 for proton over pion and kaon over pion as a function of centrality is shown in Fig. 4 (bottom). There is a trend that these ratios approach unity in more peripheral collisions indicating a better NCQ scaling behaviour.

Furthermore, the effects of partonic and hadronic scatterings on the elliptic anisotropy of final-state particles are examined in this work. Figure 5 displays the

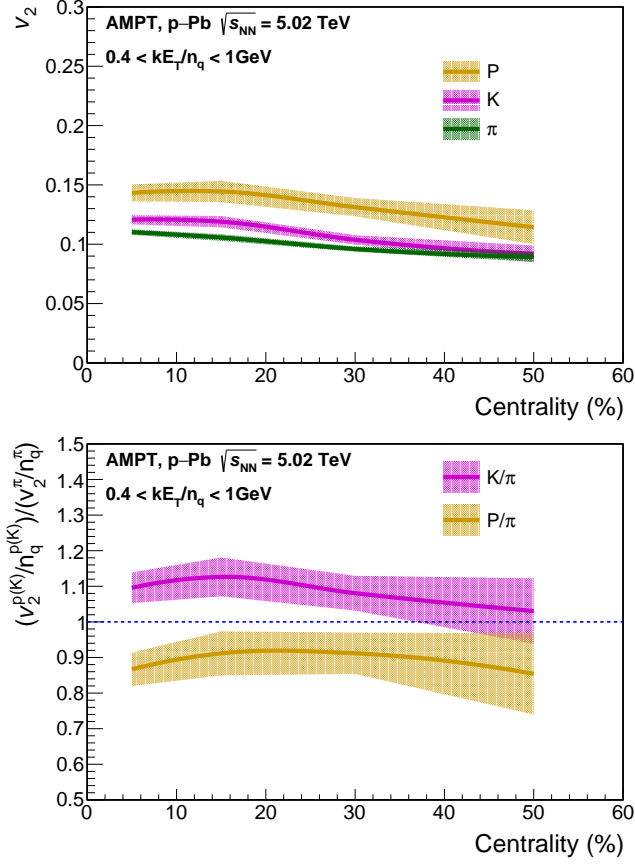


Figure 4. Top: the integrated v_2 in $0.4 < k_{E_T} < 1$ GeV for pion, kaon and proton varying with the centrality. Bottom: ratio of integrated v_2 within $0.4 < k_{E_T} < 1$ GeV for proton over pion and kaon over pion varying with the centrality.

calculated p_T -differential v_2 of pions, kaons and protons in AMPT with and without considering hadronic rescattering process in 0–20% high-multiplicity p-Pb collisions. The results show that the ratio between the v_2 values with and without hadronic rescattering is consistent with unity for all particle species, indicating that the hadronic rescattering mechanism has almost no effect on v_2 in high-multiplicity p-Pb collisions. We also investigate the centrality dependence of the hadronic rescattering effects by calculating the p_T -integrated v_2 in several centrality bins between 0–60%, as illustrated in Fig. 6. The results demonstrate that the influence of hadronic rescattering is independent of the centrality selections and has almost no impact on NCQ scaling in the range of $0.4 < k_{E_T} < 1$ GeV.

On the other hand, when we set the parton scattering cross section σ to zero, i.e., turning off the partonic scattering in AMPT, the $V_{2\Delta}$ of charged particles for central-forward (CF) and central-backward (CB) corre-

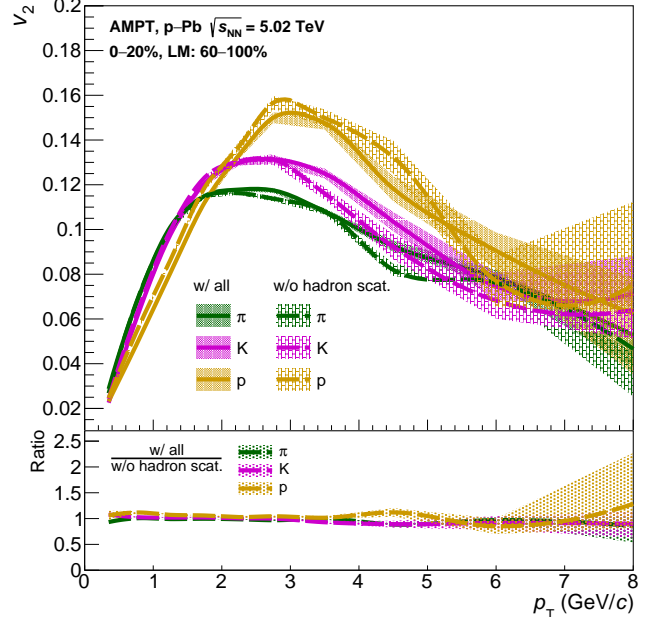


Figure 5. The p_T -differential v_2 of pions, kaons and protons calculated in AMPT model with and without considering hadronic scattering. The ratio of two sets are also presented.

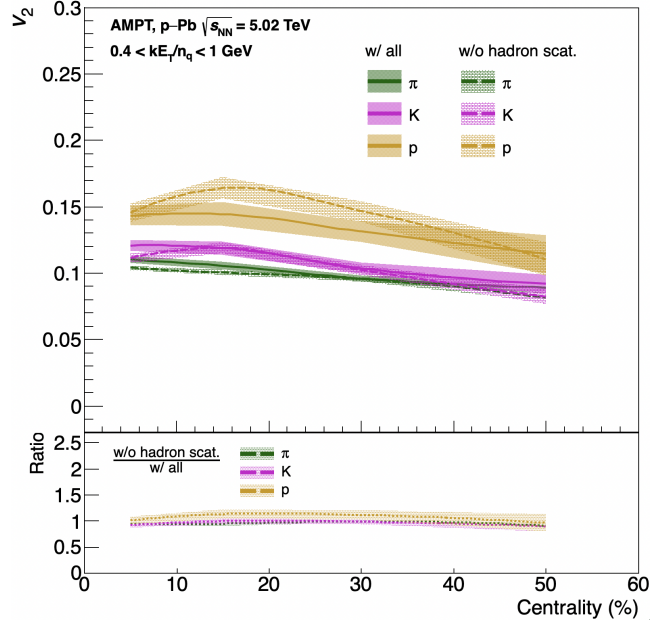


Figure 6. The integrated v_2 in $0.4 < k_{E_T} < 1$ GeV for pions, kaons and protons calculated in AMPT model with and without considering hadronic scattering. The ratio of two sets are also presented.

lations is almost zero, as demonstrated in Fig 7. This indicates that the elliptic anisotropy in high-multiplicity

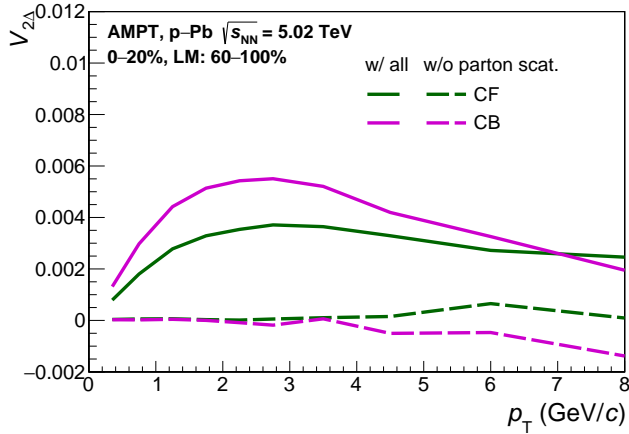


Figure 7. The p_T -differential $V_{2\Delta}$ for central-forward (CF) and central-backward (CB) correlations calculated in AMPT model with and without considering partonic scattering.

small collision systems is mostly generated by parton scatterings. Our conclusion is consistent with previous studies in AMPT [33], which suggested that few parton scatterings in small collision systems are sufficient to generate significant elliptic anisotropies through the parton escape mechanism.

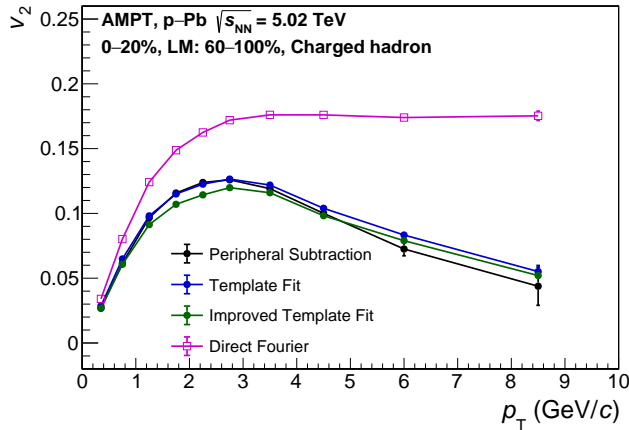


Figure 8. The p_T -differential v_2 of charged hadrons calculated in AMPT with different nonflow subtraction methods.

Finally, different nonflow subtraction methods are investigated in this paper. Figure 8 (left) shows the p_T -differential v_2 of charged particles calculated with 3×2PC method in 0–20% high-multiplicity p–Pb collisions, and several nonflow subtraction methods are implemented. In order to demonstrate how the non-

flow contribution is removed, the v_2 obtained with a direct Fourier transform of the $C(\Delta\varphi)$ correlation (as shown in Eq. 3) is also presented. The results with all subtraction methods are suppressed significantly, especially at high- p_T where the jet correlations dominate. The results obtained with peripheral subtraction and template fit are consistent, indicating that the away-side jet contribution is automatically removed with the 3×2PC method even the dependence of jet correlation on multiplicity is not considered in peripheral subtraction method. The v_2 calculated with improved template fit method is slightly lower than that from template fit, and it is similar to the features observed in ATLAS measurement [42]. Same conclusions are also obtained for the extraction of identified particle (pions, kaons, protons and Λ) v_2 .

V. SUMMARY

This study investigates the elliptic anisotropy of identified particles (pions, kaons, protons and Λ) in p–Pb collisions at 5.02 TeV using the AMPT model. We extend the calculation of v_2 to higher p_T regions, up to 8 GeV/c, using advanced nonflow subtraction techniques for the first time. We also examine the mass-ordering effect and baryon-meson grouping at low and intermediate p_T , respectively. We argue that the approximate NCQ scaling of baryon and meson v_2 can be well reproduced in $k_{ET} < 1$ GeV for several centrality bins. Furthermore, we demonstrate that parton interactions can simultaneously decrease the yield of light hadrons and generate a significant v_2 . On the other hand, hadronic rescatterings have little influence on the elliptic anisotropy of final-state particles. Thus, these findings indicate that the non-equilibrium anisotropic parton escape mechanism coupled with the quark coalescence model can also reproduce hydro-like behavior of identified particles observed in small collision systems. Overall, this study provides new insights for understanding the existence of partonic collectivity in small collision systems.

VI. ACKNOWLEDGEMENT

We thank G.L. Ma for helpful discussions. This work was supported by Natural Science Foundation of Hubei Provincial Education Department under Grant (Q20131603) and Key Laboratory of Quark and Lepton Physics (MOE) in Central China Normal University under Grant (QLPL2022P01, QLPL202106).

-
- [1] E. V. Shuryak, Phys. Lett. B **78**, 150 (1978).
 - [2] E. V. Shuryak, Phys. Rept. **61**, 71 (1980).
 - [3] J.-Y. Ollitrault, Phys. Rev. D **46**, 229 (1992).
 - [4] S. A. Voloshin, Nucl. Phys. A **827**, 377C (2009).
 - [5] S. Voloshin and Y. Zhang, Z. Phys. C **70**, 665 (1996).
 - [6] A. M. Poskanzer and S. A. Voloshin, Phys. Rev. C **58**, 1671 (1998).
 - [7] B. Alver and G. Roland, Phys. Rev. C **81**, 054905 (2010), [Erratum: Phys.Rev.C 82, 039903 (2010)].
 - [8] B. H. Alver, C. Gombeaud, M. Luzum, and J.-Y. Ollitrault, Phys. Rev. C **82**, 034913 (2010).
 - [9] G.-Y. Qin, H. Petersen, S. A. Bass, and B. Muller, Phys. Rev. C **82**, 064903 (2010).
 - [10] D. Teaney and L. Yan, Phys. Rev. C **83**, 064904 (2011).
 - [11] I. Arsene *et al.* (BRAHMS), Nucl. Phys. A **757**, 1 (2005).
 - [12] K. Adcox *et al.* (PHENIX), Nucl. Phys. A **757**, 184 (2005).
 - [13] B. B. Back *et al.* (PHOBOS), Nucl. Phys. A **757**, 28 (2005).
 - [14] J. Adams *et al.* (STAR), Nucl. Phys. A **757**, 102 (2005).
 - [15] K. Aamodt *et al.* (ALICE), Phys. Rev. Lett. **107**, 032301 (2011).
 - [16] S. Acharya *et al.* (ALICE), JHEP **07**, 103 (2018).
 - [17] G. Aad *et al.* (ATLAS), Phys. Rev. C **86**, 014907 (2012).
 - [18] S. Chatrchyan *et al.* (CMS), Phys. Rev. C **89**, 044906 (2014).
 - [19] arXiv e-prints (2022), 10.48550/arXiv.2206.04587.
 - [20] S. Acharya *et al.* (ALICE), JHEP **10**, 152 (2021).
 - [21] D. Molnar and S. A. Voloshin, Phys. Rev. Lett. **91**, 092301 (2003).
 - [22] Z.-w. Lin and D. Molnar, Phys. Rev. C **68**, 044901 (2003).
 - [23] S. Chatrchyan *et al.* (CMS), Phys. Lett. B **718**, 795 (2013).
 - [24] B. Abelev *et al.* (ALICE), Phys. Lett. B **719**, 29 (2013).
 - [25] G. Aad *et al.* (ATLAS), Phys. Rev. Lett. **110**, 182302 (2013).
 - [26] B. B. Abelev *et al.* (ALICE), Phys. Lett. B **726**, 164 (2013).
 - [27] P. Bozek, Phys. Rev. C **85**, 014911 (2012).
 - [28] P. Bozek and W. Broniowski, Phys. Lett. B **718**, 1557 (2013).
 - [29] J. L. Nagle and W. A. Zajc, Ann. Rev. Nucl. Part. Sci. **68**, 211 (2018).
 - [30] K. Dusling and R. Venugopalan, Phys. Rev. D **87**, 094034 (2013).
 - [31] K. Dusling and R. Venugopalan, Phys. Rev. D **87**, 051502 (2013).
 - [32] Z.-W. Lin, C. M. Ko, B.-A. Li, B. Zhang, and S. Pal, Phys. Rev. C **72**, 064901 (2005).
 - [33] L. He, T. Edmonds, Z.-W. Lin, F. Liu, D. Molnar, and F. Wang, Phys. Lett. B **753**, 506 (2016).
 - [34] Z.-W. Lin and L. Zheng, Nucl. Sci. Tech. **32**, 113 (2021).
 - [35] X.-N. Wang and M. Gyulassy, Phys. Rev. D **44**, 3501 (1991).
 - [36] M. Gyulassy and X.-N. Wang, Comput. Phys. Commun. **83**, 307 (1994).
 - [37] B. Zhang, Comput. Phys. Commun. **109**, 193 (1998).
 - [38] B.-A. Li and C. M. Ko, Phys. Rev. C **52**, 2037 (1995).
 - [39] L. Zheng, H. Li, H. Qin, Q.-Y. Shou, and Z.-B. Yin, Eur. Phys. J. A **53**, 124 (2017).
 - [40] N. J. Abdulameer *et al.* (PHENIX), Phys. Rev. C **107**, 024907 (2023).
 - [41] G. Aad *et al.* (ATLAS Collaboration), Phys. Rev. Lett. **116**, 172301 (2016).
 - [42] M. Aaboud *et al.* (ATLAS), Phys. Lett. B **789**, 444 (2019).
 - [43] B. B. Abelev *et al.* (ALICE), Int. J. Mod. Phys. A **29**, 1430044 (2014).
 - [44] Z.-w. Lin, S. Pal, C. M. Ko, B.-A. Li, and B. Zhang, Phys. Rev. C **64**, 011902 (2001).
 - [45] Y. He and Z.-W. Lin, Phys. Rev. C **96**, 014910 (2017).